JOURNAL OF GEOPHYSICAL RESEARCH, VOL. 102, NO. D11, PAGES 13,153–13,167, JUNE 20, 1997

# Photochemical calculations along air mass trajectories during ASHOE/MAESA

R. Bradley Pierce,[1] Jens-Uwe Grooss,[2] William L. Grose,[1] James M. Russell III,[3] Paul J. Crutzen,[4] T. Duncan Fairlie,[5] and Gretchen Lingenfelser [6]

**Abstract.** The practicality of conducting photochemical calculations along trajectories of air masses is investigated. An isentropic trajectory package is used in conjunction with a detailed photochemical model to compare predictions of the mean chemical content of air masses initialized with the Halogen Occultation Experiment (HALOE) data with coincident in situ observations from instruments onboard the ER-2 aircraft. Comparisons are made for 10 ER-2 flights originating from Christchurch, New Zealand, during the May to June and October 1994 Airborne Southern Hemisphere Ozone Experiment/ Measurements for Assessing the Effects of Stratospheric Aircraft (ASHOE/MAESA) deployments. Between 54 and 84 coincidences are found, depending on the species measured. Correlations between the ER-2 and HALOE air mass/box model calculations are high (0.56-0.90) for most species considered except for $H_2O$ (0.14) and HCl (0.24). Statistically significant low biases in the prediction of HCl, $H_2O$, and OH are found. Kolmogorov-Smirnov (KS) significance tests are used to quantify the agreement between the distribution of species observed by the ER-2 and predicted by the HALOE trajectory/ photochemical model. The model predictions agree with the observed variance within the distributions at significance levels greater than 0.80 (greater than 80% confidence that the predicted and observed variance are identical) for $H_2O$, ClO, $O_3$, and $NO_y$. The impact of computational errors in the trajectory calculations and measurement uncertainty in the computed confidence levels are investigated using Monte Carlo techniques. Computational trajectory errors are found to play a small role in reducing confidence levels. The error analysis shows that the HALOE trajectory/photochemical model calculations reproduce the large-scale variability found in the in situ ER-2 constituent measurements to within the expected uncertainties in the HALOE observations for all species considered. It is concluded that the combined trajectory/photochemical model is an effective tool for interpreting in situ aircraft observations within the global perspective provided by remote satellite measurements.

## Introduction

Satellite measurements provide a global perspective of the distribution of the average stratospheric trace gas concentrations within the finite field of view of a remote sensor. In situ high-altitude aircraft measurements provide a high-resolution perspective of the distribution of trace gas concentrations along the aircraft flight path. By effectively combining measurements from these different platforms, we can increase the spatial range of atmospheric variability which can be studied. Satellite occultation instruments have a field of view which is typically many hundreds of kilometers in the horizontal and a few kilometers in the vertical direction. Aircraft in situ measurements can be obtained at horizontal resolutions of as high as a few hundred meters. Comparisons of remote measurements with in situ measurements of relatively higher precision and accuracy provide a means of evaluating the ability of satellite measurements to characterize the average behavior of a finite air mass. In addition, the comparisons are useful for assessing the value of in situ measurements for characterizing the global distribution of atmospheric trace gases. In this investigation we examine the feasibility of using trajectory and photochemical box model calculations to compare in situ and remote measurements of photochemically active species along the aircraft flight path. Data obtained from instruments onboard the ER-2 high-altitude research aircraft during the Airborne Southern Hemisphere Ozone Experiment/ Measurements for Assessing the Effects of Stratospheric Aircraft (ASHOE/MAESA) campaign and the Halogen Occultation Experiment (HALOE) onboard the Upper Atmospheric Research Satellite (UARS) platforms are considered.

[1]NASA Langley Research Center, Hampton, Virginia.
[2]Forschungszentrum Juelich, Juelich, Germany.
[3]Hampton University, Hampton, Virginia.
[4]Max Planck Institute for Chemistry, Mainz, Germany.
[5]Science and Technology Corp., Hampton, Virginia.
[6]Science Applications International Corp., Hampton, Virginia.



Paper number 96JD03506.
0148-0227/97/96JD-03506$09.00

Most comparisons between measurements and photochemical box model predictions of the behavior of photochemically active species have been restricted to the upper stratosphere and lower mesosphere since the mixing ratios of key species such as $O_3$ are under photochemical control at these altitudes and the detailed dynamical history of the air mass is less important. Photochemical predictions of upper stratosphere and lower mesosphere $O_3$ concentrations have been extensively compared with remote sensor observations [*Natarajan and Callis*, 1989; *McElroy and Salawitch*, 1989; *Eluszkiewicz and Allen*, 1993; *Siskind et al.*, 1995], including recent comparisons with HALOE observations [*Crutzen et al.*, 1995]. Comparisons between Atmospheric Trace Molecule Spectroscopy (ATMOS) measurements and photochemical predictions for a number of species, including NO, $NO_2$, HCl, have been conducted by *Natarajan and Callis* [1991]. Comparisons with ATMOS showed that the predicted profiles were generally within the uncertainty of the observations although significant discrepancies in the sunset $NO_2$/NO ratio were found.

Photochemical model calculations were used during the European Arctic Stratospheric Ozone Experiment (EASOE) to interpret balloon, ground based, and satellite measurements of the lower stratosphere. Photochemical predictions along isentropic back trajectories originating from the EASOE observations were used to study chlorine activation [*Lutman et al.*, 1994]. Comparisons of predicted $ClO_x$ production with ClO measurements from the Microwave Limb Sounder (MLS) were in qualitative agreement, although the predicted ClO was lower than observed by MLS. Part of this difference arose because the photochemical model only accounted for the chlorine activation that occurred during the 10 day back trajectories. Photochemical studies of the effects of volcanic aerosols on $NO_x$ during EASOE were able to reproduce the vertical distribution of $NO_2$ measured by Systeme d'Analyse par Observation Zenithale (SAOZ) balloons when heterogeous chemistry on polar stratospheric cloud (PSC) and sulfate aerosols was included in the calculations [*Lateltin et al.*, 1994]. Initialization of the photochemical box model is a major uncertainty in the EASOE studies since the initial species concentrations were unknown. Photochemical box model calculations have been highly successful in reproducing the observed distribution of hydrogen, nitrogen, and chlorine radicals along ER-2 flight paths in the lower stratosphere during the Stratospheric Photochemistry, Aerosols, and Dynamics Expedition (SPADE) campaign [*Salawitch et al.*, 1994]. In these calculations the photochemical model is constrained by in situ observations of long-lived precursors, temperature, and pressure. The concentrations of diurnally varying species are then predicted by the box model. The success of these calculations demonstrates the ability of constrained photochemical models to predict much of the observed behavior of diurnally varying species.

Previous studies have demonstrated that trajectory/photochemical box model techniques can be an effective means of tracking the large-scale evolution of air masses. *Austin et al.* [1987] compared the mixing ratios of photochemically active and inert gas concentrations predicted from a coupled trajectory/photochemical model, initialized with observations from the Limb Infrared Monitor of the Stratosphere (LIMS), against subsequent LIMS observations of the same air mass. These comparisons demonstrated a sound physical basis for the use of combined trajectory/photochemical models for periods of 6 to 10 days for both disturbed and undisturbed northern hemisphere conditions. Cross correlation coefficients between modeled and observed $NO_2$ mixing ratios were significant (0.05 significance level or better) at all but the lowest isentropic level considered (500 K). $O_3$ cross correlations were not significant in the middle and lower stratosphere (below 850 K). Comparisons between initial and subsequent observations of middle stratosphere (700 K) air masses observed by HALOE during the southern hemisphere spring showed high correlations for long-lived species for periods of up to 10 days [*Pierce et al.*, 1994]. The improvement in the HALOE correlations compared to LIMS is likely a result the higher precision of the HALOE data and the use of assimilated winds instead of gradient winds derived from geopotential height data from the Stratospheric Sounding Unit (SSU). These studies establish the ability of trajectory techniques to predict the large-scale evolution of stratospheric air masses.

Taken as a whole, previous trajectory and photochemical studies show that each component of a trajectory/photochemical model can predict the behavior of the atmosphere when data at similar spatial scales are used to test and constrain the models. High-resolution in situ data from instruments onboard the ER-2 during ASHOE/MAESA and contemporaneous HALOE observations of southern hemisphere middle latitudes during 1994 provide an opportunity to quantitatively evaluate the effectiveness of using a trajectory/photochemical box model to link satellite and in situ observations of photochemically active species in the lower stratosphere. This set of observations allow us to evaluate trajectory/box model predictions, constrained by horizontally averaged satellite data and large-scale winds and temperatures, with much higher resolution in situ data. In a related paper [*Grooss et al.*, this issue] the trajectory/photochemical model is used to examine the springtime recovery of HCl in the southern hemisphere polar vortex, thereby extending observations of the Antarctic polar vortex beyond the flight range of the ER-2.

## Trajectory/Box Model Description

The trajectory model uses a fourth-order Runge-Kutta scheme with a 20 min time step to predict the displacement of air masses using linearly interpolated winds and temperatures. Winds and temperatures were obtained from operational analyses provided by the United Kingdom Meteorological Office (UKMO) (courtesy of Terry Davies) during ASHOE/MAESA. Input data for the photochemical model was saved for photochemical calculations at 1 hour increments. Trajectory/box model calculations were conducted for the second (May-June 1994) and fourth (October 1994) ASHOE deployments. These deployments correspond to periods during which the Antarctic polar vortex is developing (second deployment) and decaying (fourth deployment). During the second deployment, a total of 327 southern hemisphere HALOE occulations occurred between 940513 and 940604 (YYMMDD format is used to denote flight days)

when UKMO analysis were available for trajectory calculations. Isentropic trajectories at each HALOE observation point were initialized on the 460 K isentropic surface, which was near the mean value of the constant potential temperature leg of the ER-2 flights during this deployment. Trajectories for each occultation were predicted until 940604. Only sunset HALOE occulations were made in the southern hemisphere during May-June 1994 and those observations where restricted to middle latitudes. During the fourth deployment, a total of 471 southern hemisphere HALOE occulations occurred during the period from 940924 to 941018 for which UKMO analyses were available. Trajectories were computed on the 480 K isentropic surface during this deployment to account for the higher potential temperatures sampled by the ER-2. HALOE sunrise and sunset observations spanned the entire southern hemisphere during the fourth deployment with extensive observations within the Antarctic polar vortex. Because of operational constraints at Christchurch, New Zealand, 1200 GMT UKMO analyses were used for the trajectory calculations during the second deployment and 0000 GMT UKMO analyses were used during the fourth deployment.

The photochemical box model uses an implicit numerical integration scheme developed by *Gear* [1971] with a self-adjusting time step length. The commercial package FACSIMILE [*Curtis and Sweetenham*, 1987] is used to easily facilitate changes in reactions considered. The model includes 38 chemical species, a standard reaction scheme with 69 gas phase reactions (8 termolecular, 57 bimolecular, 4 thermal decay), including the methane oxidation chain and 22 photolysis reactions. The heterogeneous chemistry in/on ternary $H_2SO_4/HNO_3/H_2O$ solution aerosols is parameterized from results of a thermodynamic model [*Carslaw et al.*, 1995a,b] on the basis of measurements of *Hanson and Ravishankara* [1994]. Heterogeneous chemistry on crystalline NAT and ice PSCs is also incorporated. The model uses currently recommended kinetic reaction rates [*DeMore et al.*, 1994]. The photolysis rates are calculated by a spherical geometry scheme that was developed by *Lary and Pyle* [1991]. Integrations of the kinetic reaction equations are performed along a given HALOE air mass trajectory using temperature, pressure, and position information obtained from the trajectory package. For a more detailed description of the photochemical box model, see *Muller et al.*, [1993, 1994].

HALOE observations of $O_3$, $H_2O$, $CH_4$, NO, $NO_2$, and HCl are used to initialize the box model directly. Overhead column $O_3$ is held constant along the air mass trajectory and is determined from the initial HALOE sounding. The remaining species are determined from a combination of HALOE data, fixed ER-2 correlations, and monthly climatologies of the latitude-pressure distributions of species obtained from the Max Planck Institute for Chemistry (MPIC) two-dimensional model [*Gidel et al.*, 1983; *Bruhl and Crutzen*, 1993; *Grooss et al.*, 1994]. Total inorganic chlorine, $Cl_y$ ($:=HCl+ClONO_2+ClO+2Cl_2O_2+HOCl+Cl+2Cl_2$) is derived from HALOE HF data using the monthly mean relationships between HF and $Cl_y$ from the two dimensional model. A cubic polynomial fit of the two-dimensional model $Cl_y$ and HF data is used with seasonal and latitudinally dependent coefficients [*Muller et al.*, 1996]. Once $Cl_y$ has been inferred from the HALOE HF data, $ClO_x$ is obtained from the inferred $Cl_y$ minus the observed HCl. The uncertainty of this estimate of $ClO_x$ may be quite large, since it is the difference between two large quantities with both model and measurement uncertainties. The relative partitioning of ClO and $ClONO_2$ within the $ClO_x$ species is obtained from two-dimensional model climatology.

Nitrogen species are initialized using HALOE NO, $NO_2$ and the compact correlation between $NO_y$ ($:= HNO_3+NO+NO_2+NO_3+2N_2O_5+HO_2NO_2$) and $CH_4$ as measured by the reactive nitrogen and ALIAS instruments [*Fahey et al.*, 1989; *Webster et al.*, 1994]. The seasonal change in the $NO_y/CH_4$ correlation is accounted for using the $NO_y/CH_4$ correlation from a flight on 940603 for the second and the 941010 $NO_y/CH_4$ correlation for the fourth deployment. A linear least squares best fit of $NO_y$ and $CH_4$ observations from the ER-2 on these flight days is used to infer $NO_y$ from HALOE measurements of $CH_4$. $NO_y$ is the only component of the photochemical box model which is initialized with information from the ER-2 measurements. The relative partitioning between the remaining species in the $NO_y$ family (mainly $HNO_3$) is taken from two-dimensional model climatologies. *Fahey et al.* [1989] found denitrification of about 75% of the expected $NO_y$ value from mid-latitude $NO_y/N_2O$ correlations within the polar vortex during 1987 Airborne Arctic Ozone Experiment (AAOE) campaign. During the fourth ASHOE deployment, $NO_y$ concentrations within the polar vortex are reduced by 75% of the middle latitude value for the same $CH_4$ mixing ratio to crudely account for denitrification within the polar vortex. HALOE observations with $CH_4$ values of less than 1.0 ppmv at 460 K are considered to be within the polar vortex [see *Grooss et al.*, this issue, Figure 1]. Radicals with short lifetimes such as O, $O(^1D)$, OH, $HO_2$, Cl, Br, rapidly adjust themselves to photochemical equilibrium and are therefore initialized at zero concentration. All other chemical species are initialized directly from two-dimensional model climatologies.

## Determination of Coincident Pairs

Coincidence criteria of (+/-) 1 hour, 10° longitude, 1° latitude, and 20 K potential temperature were used to determine which HALOE air mass trajectories were included in the comparison with the ER-2 flight path data. These criteria result in a total of 84 coincidences, although ER-2 data for all species are not available for each flight. In situ potential temperature [*Chan et al.*, 1989] and latitude and longitude are used in conjunction with the predicted latitude and longitude to determine coincidences between the ER-2 flight path and HALOE trajectories. HALOE trajectory/box model predictions are compared with in situ measurements of nine species by instruments onboard the ER-2: HCl [*Webster et al.*, 1994], $CH_4$ [*Webster et al.*, 1994], ClO [*Anderson et al.*, 1989] $HO_2$ and OH [*Wennberg et al.*, 1995], NO and $NO_y$ [*Fahey et al.*, 1989], $O_3$ [*Proffitt et al.*, 1989] and $H_2O$ [*Kelly et al.*, 1989].

Figure 1 shows the coincident trajectories and ER-2 flight paths for each of the flights used in the comparison. Ten ER-2 flights are considered, five flights during each of the second and fourth deployments. All flights used in this compari-

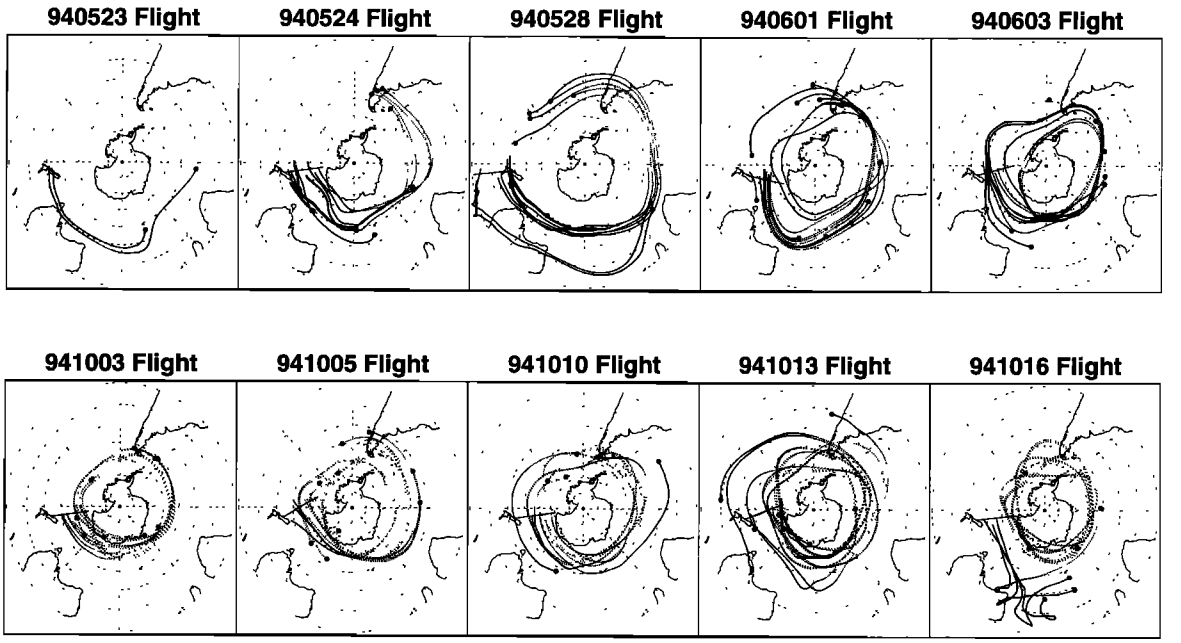


**Figure 1.** Forward trajectories (small dots) from HALOE occultation measurements (large dots) which are coincident with ER-2 flights (solid line) originating from Christchurch, New Zealand during the second and fourth 1994 ASHOE/MAESA deployments.

son originated from Christchurch, New Zealand and sampled mid-latitude and vortex edge air masses with the exception of the 940528 flight during the second deployment which sampled subtropical air masses. During the second deployment (flight days 940523, 940524, 940528, 940601, 940603), coincident trajectories are restricted to mid-latitude orbits on the equatorward flank of the polar night jet and originate from mid-latitude HALOE observations. During the fourth deployment (flight days 941003, 941005, 941010, 941013, 941016), more coincidences occur near the edge of the polar vortex, and some of the coincident trajectories originate from subtropical HALOE observations (flight days 941013, 941016). Figure 2 shows the observed $O_3$ mixing ratios along the ER-2 flight path together with the predicted $O_3$

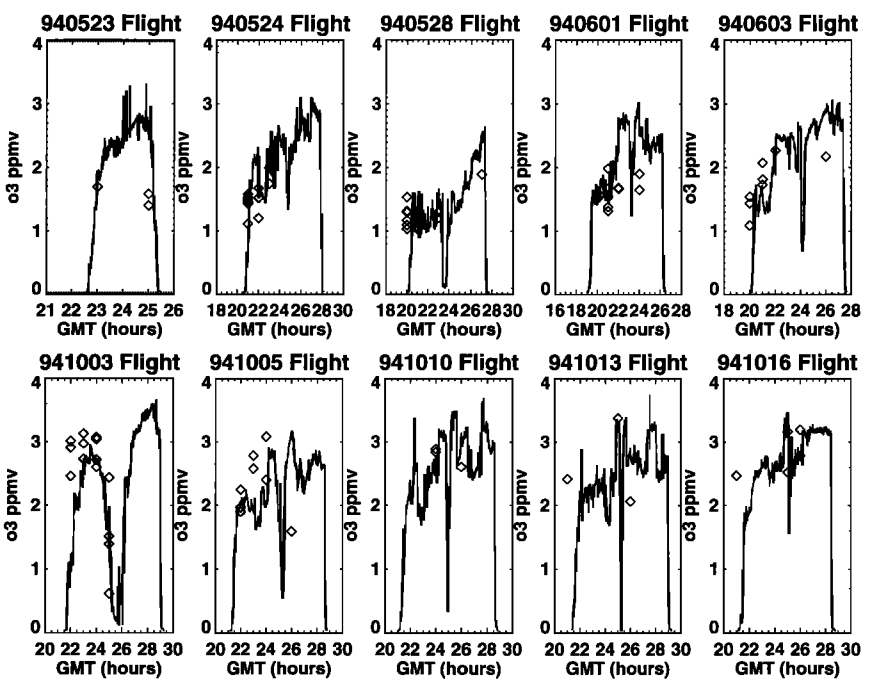


**Figure 2.** In situ measurements of $O_3$ mixing ratio (solid line) sampled at 1Hz by the NOAA Aeronomy Laboratory dual-beam UV-absorption ozone photometer (courtesy of Mike Proffitt) and predicted $O_3$ mixing ratios for coincident trajectories (diamonds) for each flight shown in Figure 1.

mixing ratios for coincident trajectories from the HALOE trajectory/box model for each flight. The ASHOE/MAESA ER-2 flights typically began between 2000 GMT and 2200 GMT, (0600 and 0800 LT) and include an isentropic southbound leg, a dive between 2400 GMT and 2600 GMT (1200 and 1400 LT) and then a cruise climb during the northbound return leg. Most coincidences occur during the southbound isentropic leg of the flight. Qualitatively, the agreement between the predicted and the observed $O_3$ mixing ratios appears to be quite good inspite of the significant small-scale variability of the in situ ER-2 data. These figures illustrate the wide range of observed and predicted $O_3$ mixing ratios sampled during the two deployments.

The small-scale variability in the in situ ER-2 measurements arises due to a combination of large-scale chaotic advection [*Pierce and Fairlie*, 1993], resulting in the development of thin filaments of air of vortex and subtropical origin in close proximity and differential advection by small-scale disturbances such as gravity waves [*Pfister et al.*, 1993; *Bacmeister et al.*, 1996]. Because of the chaotic nature of the large-scale filamentation process and the inability to resolve small-scale disturbances in global analyses of wind and temperature, it is unlikely that the HALOE trajectory/box model predictions can account for the detailed structure observed by the ER-2. Therefore we restrict ourselves to a comparison between the HALOE trajectory/box model predictions and the mean ER-2 mixing ratios within the coincidence window. Averaging the ER-2 flight track data within the coincidence window results in a set of prediction/observation pairs for each flight. The resulting predicted and observed samples have an equal number of data points, which greatly simplifies the statistical analysis. In the following discussion, "observed ER-2 data" will refer to the average ER-2 mixing ratio within the coincidence window unless otherwise stated.

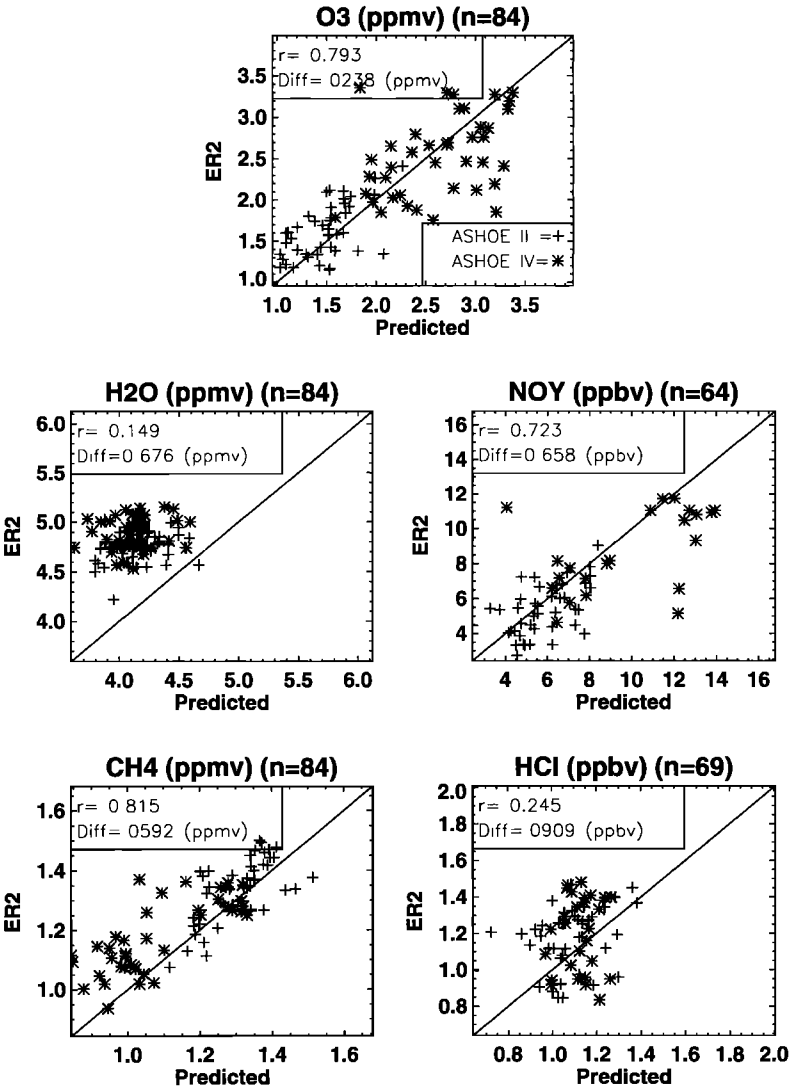


**Figure 3.** Scatterplots of observed (ER-2) and predicted HCl, $H_2O$, $O_3$, $NO_y$, and $CH_4$ mixing ratios for coincident trajectories during the second (+) and fourth (*) deployments. Cross-correlation coefficients (r) and mean differences (Diff) are indicated in the top left corner for each constituent. The number of coincident pairs (n) for each constituent is also indicated. In situ data are provided by Chris Webster (HCl, $CH_4$), David Fahey ($NO_y$), Mike Proffitt ($O_3$), and Ken Kelly ($H_2O$). The in situ data have been averaged within the coincident window to facilitate intercomparison.

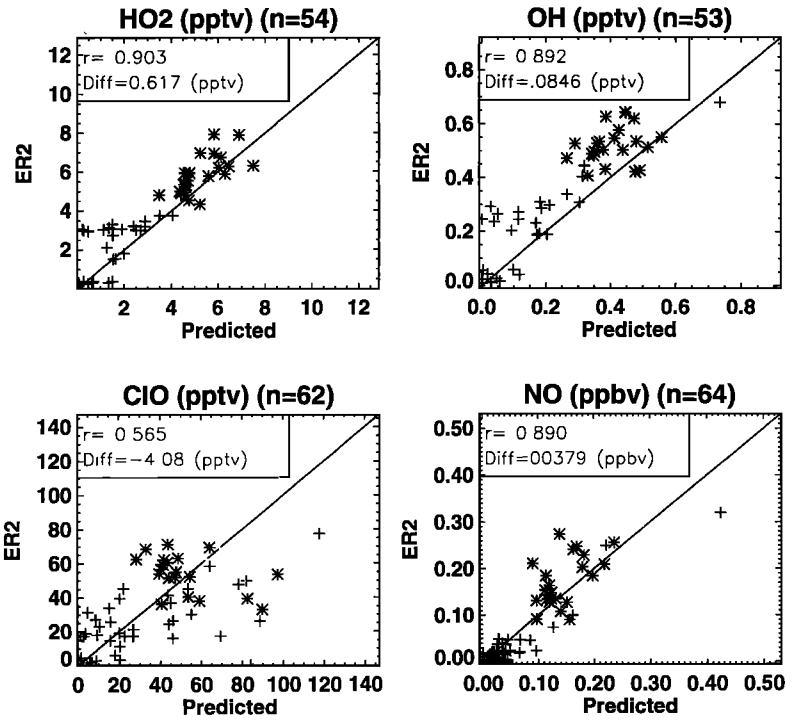


**Figure 4.** Scatterplots of observed (ER-2) and predicted $HO_2$, ClO, OH, and NO mixing ratios for coincident trajectories during the second (+) and fourth (*) deployments. Cross-correlation coefficients (r) and mean differences (Diff) are indicated in the top left corner for each constituent. The number of coincident pairs (n) for each constituent is also indicated. In situ data are provided by Jim Anderson (ClO), Paul Wennberg (OH and $HO_2$), and David Fahey (NO). The in situ data have been averaged within the coincident window to facilitate intercomparison.

Averaging within the coincidence window typically results in a 2° latitude average along ER-2 flight track due to the predominately north/south orientation of the flight tracks.

## Statistical Analysis

The number of coincident pairs during each flight was considered too small for reliable flight-by-flight statistical comparison. Instead, the coincident pairs for all flights (both second and fourth deployments) were combined into one sample. This increases the range of atmospheric variability included in the statistical samples and allows us to evaluate whether the HALOE trajectory/box model predictions can account, in an average sense, for the range of behavior observed by the ER-2 during dynamically active southern hemisphere early winter and spring periods.

Scatterplots of the observed and predicted concentrations of long-lived species ($O_3$, $H_2O$, $NO_y$, $CH_4$, and HCl) for both the second and the fourth deployments are shown in Figure 3. Scatter plots of the observed and predicted concentrations of diurnally varying species ($HO_2$, OH, ClO, NO) are shown in Figure 4. Both observed and predicted concentrations of $O_3$ and $NO_y$ were higher, while the concentration of $CH_4$ was generally lower during the fourth deployment. This indicates that the concentration of long-lived species such as $O_3$, $CH_4$, and $NO_y$ are being controlled by seasonal descent of mid-latitude air which brings higher concentrations of $O_3$ and $NO_y$ and lower concentrations of $CH_4$ down to ER-2 altitudes. Water vapor and HCl have much weaker vertical gradients in mid-latitudes and consequently do not show significant seasonal trends. The observed increase in $O_3$ and $NO_y$ and constant $H_2O$ suggests that the coincident air masses observed during October were not significantly affected by heterogeneous polar processes, which would have led to $NO_y$ and $H_2O$ reductions due to PSC sedimentation, and reductions in $O_3$ due to chlorine-catalyzed ozone destruction. The observed and predicted increase in the photochemically active species ($HO_2$, ClO, OH, NO) between the second and the fourth deployments arises from seasonal changes in the solar zenith angle of the coincident air masses. The agreement between the trends in the observed and predicted concentrations demonstrates the ability of the HALOE trajectory/box model to predict the temporal behavior of both long-lived and diurnally varying species.

### Cross correlations and mean differences

Cross-correlation coefficients (r) and mean differences (observed-predicted) for the combined data sets were computed for the coincident observation/prediction pairs. These are indicated for each species in Figures 3 and 4. Observed and predicted $HO_2$, OH, NO, $O_3$, $CH_4$, and $NO_y$ concentrations are all highly correlated, while the predicted and observed ClO are reasonably well correlated. The reduced correlation for ClO may be due to the lower signal to noise ratio of the ER-2 observations for the low ClO mixing ratios

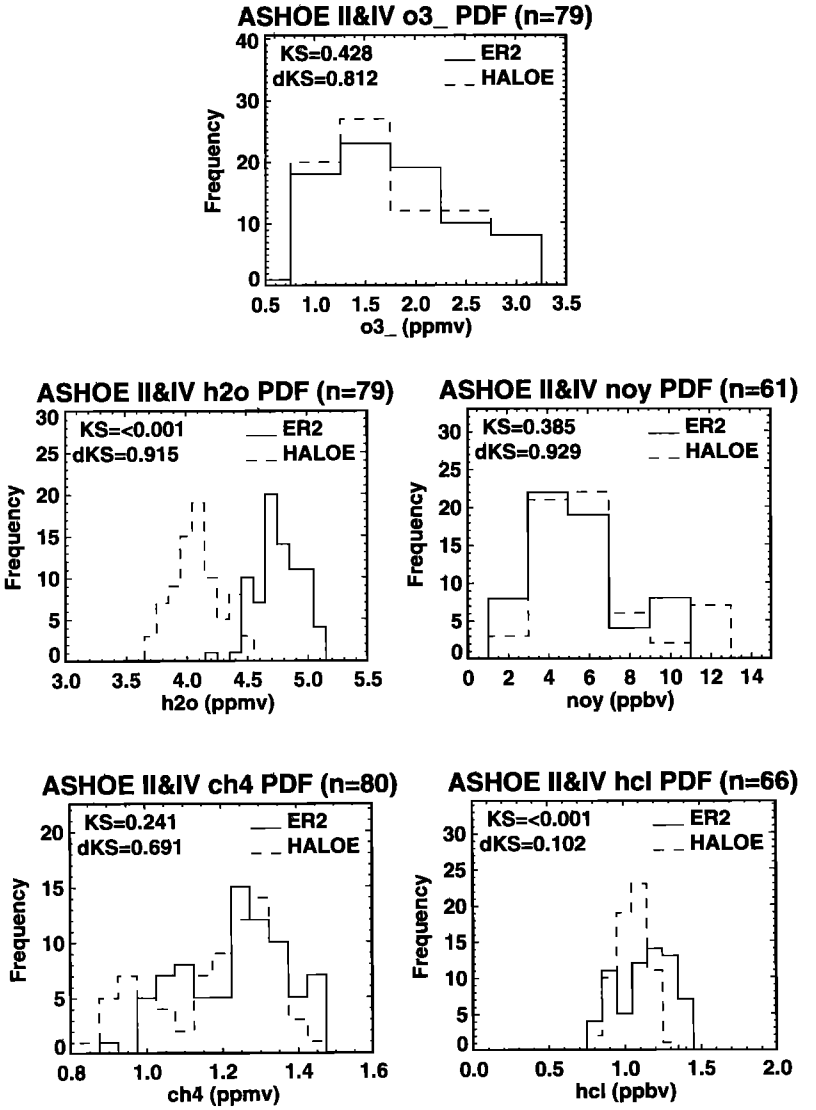


**Figure 5.** Probability density distributions (PDFs) of observed (solid line) and predicted (dashed line) HCl, $H_2O$, $O_3$, $NO_y$, and $CH_4$ mixing ratios for coincident trajectories during the second and fourth deployments. Kolmogorov-Smirnov (KS) significance levels with (KS) and without (dKS) mean differences in the observed and predicted mixing ratios are indicated in the top left corner for each constituent. The number of coincident pairs (n) for each constituent is also indicated.

in the coincident air masses. Water vapor and HCl comparisons show poorer correlations. The low correlations for $H_2O$ and HCl arise partly because of the small range of variability in these species for the coincident air masses. Significance levels for the correlation coefficients were determined using the Student's $T$ test. The correlation coefficients are statistically significant at the 0.05 significance level for all species except for $H_2O$.

The statistical significance of the agreement between the mean concentrations was determined using the Mann-Whitney ranked sum (RS) test of means [*Pratt and Gibbons*, 1981]. The HALOE trajectory/box model predictions of mean $O_3$, ClO, NO, $HO_2$, and $NO_y$ concentrations are significant at the 0.05 significance level. RS significances for HCl, $H_2O$, $CH_4$, and OH are less than 0.05 and indicate statistically significant low biases for these species.

### Kolmogorov-Smirnov significance tests

The Kolmogorov-Smirnov (KS) test [*Gibbons*, 1985] is used to determine the likelihood that the observed and predicted mixing ratio distributions arose from the same parent population. The Kolmogorov-Smirnov test is similar to the more familiar chi-squared test except that the maximum difference between the two sample's cumulative probability density function (PDF) is used instead of the maximum difference between the PDFs. The KS statistic provides a more quantitative measure of the agreement between the predicted and the observed mixing ratios than either the Student's $T$ or RS tests provide. To compute the cumulative PDFs, we follow *Gibbons* [1985]. The KS significance is obtained from an asymptotic approximation for the exact two-sided KS null distribution which is valid for large n [*Pratt and Gib-*

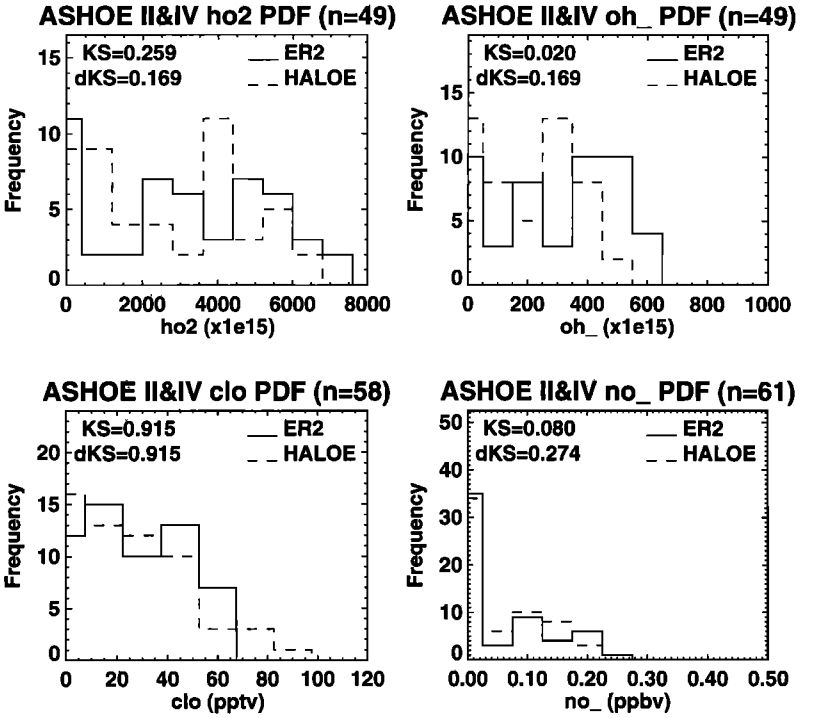


**Figure 6.** PDFs of observed (solid line) and predicted (dashed line) $HO_2$, ClO, OH, and NO mixing ratios for coincident trajectories during the second and fourth deployments. Kolmogorov-Smirnov (KS) significance levels with (KS) and without (dKS) mean differences in the observed and predicted mixing ratios are indicated in the top left corner for each constituent. The number of coincident pairs (n) for each constituent is also indicated.

*bons*, 1981]. Because the KS test is sensitive to outlying data points, we removed those ER-2 and HALOE trajectory/box model pairs which lie more than 2 standard deviations from the linear best fit of the data shown in Figures 3 and 4. This results in the loss of no more than 3 to 5 coincidence pairs, depending on the species considered.

Figures 5 and 6 show predicted and observed mixing ratio PDFs and KS significance levels (KS) for each constituent during the second and fourth deployments. KS significance levels are also shown after the mean biases between the predicted and the observed concentrations have been removed (dKS). Both observed and predicted distributions of photochemically fast species such as $HO_2$ and OH show very broad distributions with no single clear peak. This reflects the wide range of local zenith angles sampled along the ER-2 flight path during the second and fourth deployments. The NO distribution shows a strong peak at low NO mixing ratios in both the observed and the predicted distributions. The low NO mixing ratios were observed during the second deployment. Two-dimensional model calculations of the diurnal cycle of NO and OH [*M. Natarajan*, personal communication, 1996] indicate that the differences between the OH and the NO distributions can be accounted for by differences in the early morning increases in these constituents. During May at 56° S, NO concentrations show a relatively slow early morning rise from 0.0 ppbv to maximum near 0.1 ppbv by noon (time period for isentropic leg of ER-2 flights), while OH concentrations show a relatively rapid morning rise from 0.0 pptv to 0.25 pptv by noon. Consequently, there is a high likelihood of sampling very low NO and intermediate OH (and intermediate $HO_2$) mixing ratios during the second deployment. The predicted distributions of $O_3$, $NO_y$, and ClO are in good qualitative agreement with the observed distributions. The predicted and observed distributions of these species are all skewed toward lower mixing ratios due to the frequent sampling of mid-latitude air masses (with lower mixing ratios) and less frequent sampling of more poleward air (with higher mixing ratios). Both the observed and the predicted $CH_4$ distributions are bimodal with a secondary peak at lower $CH_4$ mixing ratios. The secondary peak in the HALOE PDF occurs at mixing ratios between 0.9 and 1.0 ppmv, while the secondary peak in the ER-2 PDF occurs at mixing ratios between 1.0 and 1.1 ppmv. The bimodal PDFs arise from flights during the fourth deployment where filaments of vortex air were frequently encountered in middle latitudes. The HALOE $CH_4$ was lower than the ER-2 $CH_4$ in these vortex filaments. There is a qualitative disagreement between the shape of the predicted and observed distributions of HCl with a much wider range of observed HCl mixing ratios than is predicted. Predicted HCl tendencies were low for the coincident trajectories, so these differences most likely reflect the relatively coarse vertical resolution (3 km) of the HALOE HCl retrievals used to initialize the box model. The mean $H_2O$ bias is quite evident in the histograms although the predicted distribution appears to capture the variance of the observed $H_2O$ distribution reasonably well.

The predicted and observed PDFs agree at 0.05 significance level for $HO_2$, ClO, $O_3$, $NO_y$, $CH_4$, and NO. This is

consistent with the results of the Student's $T$ and RS tests except for $CH_4$, which showed a statistically significant mean low bias in the RS test. The RS test only measures the agreement between the means of the distributions, while the KS test measures the agreement between the overall distributions. The bimodal nature of the $CH_4$ PDFs suggests that a single mean does not adequately represent the distribution of $CH_4$ mixing ratios, and consequently the KS test is a more robust estimate. The predicted and observed PDFs disagree at the 0.05 significance level for HCl, $H_2O$, and OH. This disagreement is due to low biases in the predicted distributions since these species also failed the Mann-Whitney test of equal means. The actual KS significance is generally less than 0.50, and consequently there is a strong likelihood (greater than 50%) that the predicted and observed distributions are not identical. The ClO prediction shows the highest significance level (0.915) in spite of the large uncertainties in the initial $ClO_x$ partitioning during the box model initialization.

KS significance is, in general, much higher when the mean biases between the predicted and observed distributions are removed. Only $HO_2$ shows a dKS significance which is less than its KS significance. This counterintuitive result can occur if mean errors are acting to offset rms errors in the $HO_2$ prediction. The dKS significances indicate that the variance within the predicted and observed distributions are identical at the 0.05 significance level for all species. Actual dKS significance levels are greater than 0.80 for $H_2O$, ClO, $O_3$, and $NO_y$. The large difference between the KS and dKS significance for $H_2O$ can be understood from the statistically significant low bias found for $H_2O$. The large differences between KS and the dKS for $O_3$ and $NO_y$ indicate that even small biases in these species can have a large impact in the computed KS significance levels.

Table 1 summarizes the results of the statistical tests with the combined data sets and also presents results for the second and fourth deployments. For the combined data sets the Student's $T$, Mann-Whitney, and KS tests all support the hypothesis that for coincident air masses the distribution of $HO_2$, ClO, $NO_y$, and NO mixing ratios predicted by the HALOE trajectory/photochemical box model are identical to the distribution observed by the ER-2 (averaged within the coincidence window) at the 0.05 significance level. The dKS tests support the hypothesis that the predicted and observed variances are identical for all species considered. The Mann-Whitney and KS tests establish with 95% confidence that there is a mean low bias in the predicted concentrations of HCl, $H_2O$, and OH mixing ratios. The Student's $T$ and KS tests indicate that the predicted and observed $CH_4$ distributions are identical at the 0.05 significance level although the Mann-Whitney test indicates a statistically significant low bias in the HALOE $CH_4$. The disagreement between the KS and the Mann-Whitney tests for $CH_4$ are most likely due to the bimodal nature of the $CH_4$ distribution. The agreement between the observed and the predicted distributions appears to be somewhat better during the fourth deployment than the second: dKS significance for $O_3$ and OH were greater than 0.95 during the fourth deployment; $HO_2$, $O_3$, ClO, $CH_4$, and OH dKS significance were all much higher during the fourth deployment than during the second deployment; and only HCl, $H_2O$, and NO dKS significance were much higher during the second deployment than during the fourth deployment. However, the number of coincident observations during the fourth deployment was considerably less than dur-

**Table 1.** Summary of Statistical Analysis for the Second Deployment (ASHOE II), Fourth Deployment (ASHOE IV), and Combined Samples (ASHOE II and IV)

| | ASHOE II | | | | | ASHOE IV | | | | | ASHOE II and IV | | | | |
|---|---|---|---|---|---|---|---|---|---|---|---|---|---|---|---|
| | n | r | dx | KS | dKS | n | r | dx | KS | dKS | n | r | dx | KS | dKS |
| $HO_2$ | 34 | 0.62 | 658. | 0.01 | 0.04 | 22 | 0.66 | 556. | 0.04 | 0.84 | 54 | 0.90 | 617 | 0.26 | 0.17 |
| HCl | 42 | 0.32 | 0.10 | 0.01 | 0.40 | 27 | 0.09 | 0.08 | 0.01 | 0.05 | 69 | 0.24 | 0.09 | 0.0 | 0.10 |
| $H_2O$ | 45 | 0.21 | 0.59 | 0.0 | 0.45 | 39 | 0.16 | 0.77 | 0.0 | 0.20 | 84 | 0.14 | 0.67 | 0.0 | 0.92 |
| ClO | 42 | 0.62 | -6.9 | 0.76 | 0.16 | 20 | 0.46 | 1.9 | 0.07 | 0.30 | 62 | 0.56 | -4.0 | 0.92 | 0.92 |
| $O_3$ | 44 | 0.58 | 0.12 | 0.12 | 0.62 | 40 | 0.43 | -0.10 | 0.54 | 0.98 | 84 | 0.79 | 0.02 | 0.43 | 0.81 |
| OH | 31 | 0.83 | 63.0 | 0.56 | 0.11 | 22 | 0.24 | 114. | 0.0 | 0.98 | 53 | 0.89 | 84. | 0.02 | 0.17 |
| $NO_y$ | 42 | 0.52 | -0.42 | 0.15 | 0.91 | 22 | 0.49 | -1.1 | 0.04 | 0.84 | 64 | 0.72 | -0.65 | 0.39 | 0.93 |
| NO | 42 | 0.94 | -0.02 | 0.03 | 0.75 | 22 | 0.52 | 0.03 | 0.36 | 0.19 | 64 | 0.89 | 0.0 | 0.08 | 0.27 |
| $CH_4$ | 45 | 0.67 | 0.03 | 0.06 | 0.42 | 39 | 0.74 | 0.09 | 0.01 | 0.54 | 84 | 0.82 | 0.06 | 0.24 | 0.69 |

n = number of coincident trajectories, r = cross correlation coefficients,(dx)= mean differences, KS = Kolmogorov-Smirnov significance levels, and dKS = Kolmogorov-Smirnov significance levels with mean differences removed for observed (ER-2) and predicted $HO_2$(x1e15), HCl (ppbv), $H_2O$(ppmv), ClO (pptv), $O_3$(ppmv), OH (x1e15), $NO_y$(ppbv), NO (ppbv), and $CH_4$(ppmv) mixing ratios.

ing the second deployment. KS significance levels are very sensitive to the number of data points so that comparison between the two deployments should be approached with caution.

## Error Analysis

The computed KS and dKS significance levels, while high enough to support agreement between the predicted and the observed distributions, are not high enough to establish with a greater than 95% confidence that the two distributions are equal. Therefore it is useful to examine the impact of known error sources on the KS significance levels to determine whether we can account for the computed levels of significance. The impact of numerical trajectory errors and HALOE measurement uncertainty are investigated here. The sensitivity of the photochemical box model calculations to assumptions regarding the extent of denitrification, aerosol amount and partitioning within the $ClO_x$ species are discussed by *Grooss et al.*, [this issue].

### Numerical trajectory errors

The impact of numerical trajectory errors in the photochemical predictions was investigated in a case study for the 941016 flight. In this case study we investigate the impact of displacement errors in the ability of the trajectory package to predict the distribution of potential vorticity (PV) on the 480 K isentropic surface. Since PV is largely conserved at ER-2 altitudes, it can be treated as a tracer, and the distribution of PV should provide a reasonable representation of the distribution of the longer-lived species considered in this intercomparison. A grid of 2000 parcels was initialized at 0000 GMT on 941016 in the neighborhood of the ER-2 flight track with 0.1° meridional spacing between 45° S and 65° S and 1° longitudinal spacing between 165° E and 175° E. Fifteen day backtrajectories were computed for each parcel. Forward trajectories originating at the parcel's location at 0000 GMT for each day of the backtrajectory were then computed. These simulations provide us with a set of 15 backward/forward forecasts of the initial parcel location which range in length from 2 to 30 days. Each parcel was initialized with PV at the parcel's location which was derived from UKMO analyzed winds and temperatures. The PV at the initial parcel location on 941016 is considered the "truth." The analyzed PV at the predicted parcel location is considered the "predicted" PV. Differences between the predicted and the true PV arise due to errors in the predicted location of the parcels. The displacement errors in this case study can only be caused by numerical errors in the trajectory calculation since identical winds are used in the backward and forward trajectories, and the same distribution of PV is used for both true and predicted PV samples.

Monte Carlo simulations were conducted to determine the impact of numerical trajectory errors on the computed KS statistics by extracting 100 random samples out of the true and predicted PV distributions for each backward/forward forecast. Sample sizes of 10, 100, and 1000 were considered. Figure 7 shows the resulting expected KS significance as a function of the age of the air mass for the three sample sizes. The vertical bars indicate the standard deviation of

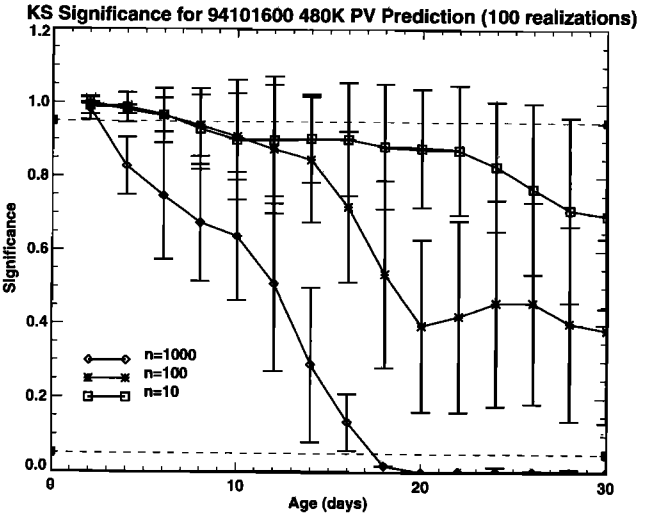


**Figure 7.** Expected Kolmogorov-Smirnov (KS) significance levels as a function of age of the trajectory due to computational errors in the trajectory calculation. One hundred Monte Carlo predictions of the distribution of potential vorticity in the neighborhood of the ER-2 flight path on 941016 were conducted for each age. Mean KS significance are shown for three different sample sizes (n=10 squares; n=100 asterisk, and n=1000 diamonds). The standard deviation of the Monte Carlo simulations are denoted by vertical bars.

the KS significance levels found in the Monte Carlo simulation for each parcel age. For small sample sizes (n=10) the expected KS significance decreases slowly to about 0.75 for 30 day trajectories. The 0.95 significance level is within the standard deviation of KS significance for small sample sizes out to 30 days. For intermediate sample sizes (n=100) the expected KS significance is within 1 standard deviation of the 0.95 significance level out to 14 days and then drops quickly down to near 0.40. For large sample sizes (n=1000) there is a nearly uniform reduction of the expected KS significance until they drop below the 0.05 significance level at day 18. The n=100 sample size is most representative of the number of HALOE trajectory/box model and ER-2 coincidences found during the second and fourth deployments. Therefore for the sample sizes considered, this case study suggests that numerical trajectory errors did not make a significant impact on the computed statistics for trajectories less than 15 days old. However, if larger samples had been obtained, numerical trajectory errors could lead to a large reduction in the statistical significance of the agreement between computed and predicted distributions of long-lived species.

Coincident trajectories range in age from 13 hours to 20 days, 11 hours with a distribution which is skewed toward shorter times (not shown); 78.5% of the coincident trajectories are less than 15 days old, and 61.9% are less than 10 days old. Monte Carlo simulations were conducted to estimate the impact of numerical trajectory errors on the expected KS significance for the distribution of ages for coincident trajectories. KS significance tests were applied to 100 random samples of size n=84 (the number of coincident trajectories) of the true and predicted PV distributions. The random samples were constructed by sampling each forecast

using the number of coincident parcels with ages equal to the individual PV forecast's length to determine the number of times each forecast was randomly sampled. With this procedure, each sample PV forecast within the Monte Carlo simulations has an age distribution which is equal to the age distribution of the coincident trajectories in the combined ER-2/HALOE data set. The Monte Carlo simulations show that when the distribution of ages in the coincident trajectories are considered, the expected KS significance for the agreement between the true and predicted PV is 0.889(+/-) 0.005 for typical numerical trajectory errors. These numerical trajectory errors provide an upper limit to the confidence level of the trajectory/box model predictions which is somewhat below the 0.95 significance level.

### HALOE measurement uncertainties

HALOE measurement uncertainties contribute to errors in the trajectory/box model predictions for long-lived species such as HCl, $H_2O$, $O_3$, $CH_4$, and $NO_y$ and for photochemically active species such as NO (for short trajectories) due to errors in the box model initialization. A comprehensive program has been carried out by the HALOE science team to estimate errors and validate HALOE data through Monte Carlo analyses and comparisons with correlative measurements. Estimates of random errors include instrument noise, pointer/tracker noise, and random errors in the retrieval of interfering gases (e.g., $CH_4$ and $H_2O$ in the HCl channel). Systematic errors considered include radiance calculation errors, bias due to removal of electronic effects in the data, temperature/pressure uncertainty, and biases due to systematic errors in interfering gases. The estimated accuracies (combination of random and systematic uncertainty) in the lower stratosphere are 20% for HCl [*Russell et al.*, 1996], 10% for $H_2O$ [*Harries et al.*, 1996], 15% for $O_3$ [*Bruhl et al.*, 1996], 20% for $CH_4$ [*Park et al.*, 1996], and 25% for NO [*Gordley et al.*, 1996].

The impact of measurement errors on the confidence in the prediction will vary depending on the species considered because of the different characteristics of the distribution observed by the ER-2 for each constituent. Monte Carlo simulations were conducted to examine the impact of uncertainty in the HALOE observations on the computed KS significance levels. In these experiments, random errors with rms values ranging from 5 to 50% (1 to 10% for $H_2O$) were introduced into the observed (ER-2) distribution for each constituent. This observed plus random error sample serves as a proxy for HALOE observations with a prescribed rms error ampli-

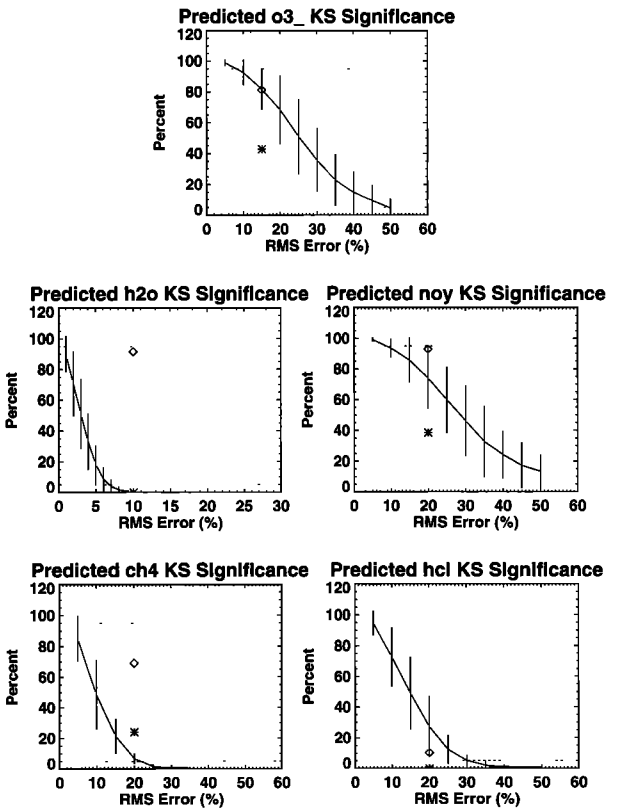


**Figure 8.** Expected Kolmogorov-Smirnov (KS) significance levels (solid line) and standard deviations (vertical bars) due to HALOE measurement uncertainty as a function of the rms amplitude of imposed random errors for HCl, $H_2O$, $O_3$, $NO_y$, and $CH_4$. The computed KS (asterisk) and dKS (diamond) significance are also shown. The rms error associated with the computed KS and dKS significance is the quoted HALOE measurement uncertainty. One hundred Monte Carlo estimates of the KS significance levels were determined for each specie and rms error amplitude by introducing random errors into the observed (ER-2) mixing ratio.

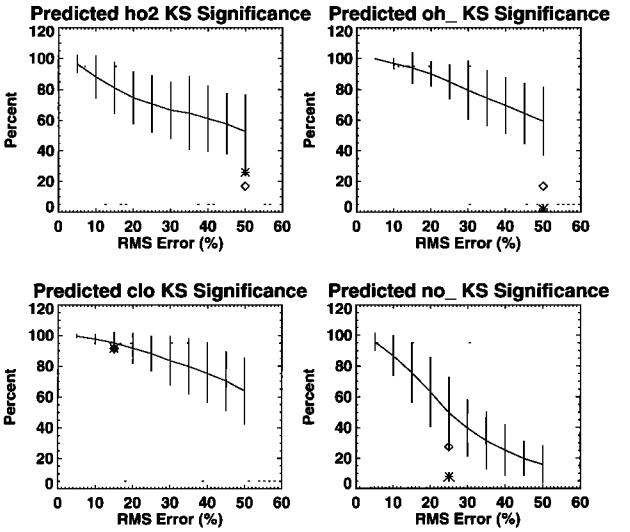


**Figure 9.** Expected Kolmogorov-Smirnov (KS) significance levels (solid line) and standard deviations (vertical bars) due to HALOE measurement uncertainty as a function of the rms amplitude of imposed random errors for $HO_2$, ClO, OH, and NO. The computed KS (asterisk) and dKS (diamond) significance are also shown. For NO the rms error associated with the computed KS and dKS significance is the quoted HALOE measurement uncertainty. For species predicted by the photochemical model ($HO_2$, ClO, OH) the rms error associated with the computed KS and dKS uncertainty is 50% or less depending on whether the computed significance levels fall within one standard deviation of the expected mean KS. One hundred Monte Carlo estimates of the KS significance levels were determined for each specie and rms error amplitude by introducing random errors into the observed (ER-2) mixing ratio.

tude. An "expected" KS significance level was determined using 100 samples for each rms error value for each species. Figures 8 and 9 show the expected KS significance level as a function of rms error for each species considered. The standard deviations of the Monte Carlo simulations are indicated by vertical bars. The computed KS and dKS significance levels (from Figures 5 and 6) are also shown.

The rms error for the computed KS and dKS significance level is the quoted HALOE uncertainty for HCl, $H_2O$, $O_3$, $CH_4$, $NO_y$ (using HALOE $CH_4$ uncertainties), and NO. The rms errors for those species not measured by HALOE ($HO_2$, ClO, OH) are equal to the lowest rms error with expected KS significance within (+/-) 1 standard deviation of the computed KS significance, or 50%, whichever is the smaller, and therefore provide an estimate of the rms error in the predicted mixing ratio for these species.

As discussed earlier, $HO_2$, ClO, and OH have relatively broad distributions. This feature makes these constituents relatively insensitive to rms errors in the prediction as indicated by the gradual decrease in the expected KS significance levels with increasing rms error. $O_3$ and $NO_y$ show intermediate decreases, while HCl, $CH_4$, and $H_2O$ are the most sensitive to rms errors due to the narrow range of observed mixing ratios and the bimodal nature of the $CH_4$ mixing ratio distribution. Consequently, the expected KS significance for HCl, $CH_4$, and $H_2O$ decreases rapidly with increasing rms errors.

The dKS significance level is the most appropriate statistic to compare with the expected KS significance since there was no mean bias imposed in the Monte Carlo simulations. Computed dKS significance for all species observed by HALOE are within 1 standard deviation of the expected KS significance or better for the quoted HALOE uncertainties, although the computed dKS uncertainty for NO is near the minimum expected KS significance for a 25% error. HALOE measurement uncertainty does not fully account for the computed KS significance level for NO because this gas has a large diurnal variation and most trajectories are longer than 1 day. These results indicate that the computed levels of KS significance for the predicted distributions of $H_2O$, HCl, $O_3$, $NO_y$, $CH_4$, and NO are primarily determined by uncertainties in the initial HALOE measurement. The computed KS significance for ClO is consistent with a 15% rms error in the ClO prediction. The computed KS and dKS significance for $HO_2$ and OH indicate that the rms errors in predictions of these species are larger than 50%.

## Case Study for 941010 Flight

To illustrate the utility of the HALOE air mass/photochemical box model calculations in characterizing the distribution of stratospheric trace species, we present a case study for the flight of 941010. This southbound flight out of Christchurch, New Zealand, extended to nearly 70° S, encountering the edge of the polar vortex at the southern-most portion of the outbound flight leg (see Figure 1). HALOE made extensive measurements within the Antarctic vortex prior to 941010. The HALOE air mass/photochemical calculations allow us to map these observations forward in time to 941010 and extend the latitude range of southern hemisphere observations beyond what is available from in situ measurements. Predicted concentrations of trace species on the 480 K isentropic surface at 0000 GMT on 941010 in a longitude band between 150° E and 150° W were selected for this case study.

Plate 1 shows the observed and predicted distributions of HCl, $O_3$, $H_2O$, ClO, and inferred distributions of $Cl_y$ and $ClONO_2$ plotted as a function of latitude. Only the southbound, constant potential temperature leg of the ER-2 flight is shown. The ER-2 data has been restricted to those observations with potential temperatures between 460 K and 500 K. The ER-2 $Cl_y$ is inferred from ATLAS $N_2O$ [*Loewenstein et al.*, 1989] following the procedure described by *Webster et al.*, [1993]. $ClONO_2$ is inferred from the difference between $Cl_y$ and HCl+ClO for both the ER-2 and the HALOE air mass/photochemical box model. The edge of the polar vortex is located at approximately 70° S at the longitude of the flight on 941010. During this flight the ER-2 encountered a filament of air near 50° S which had originated from the edge of the polar vortex [see *Fairlie et al.*, this issue, Figure 1]. This filament is seen as a narrow peak of high $O_3$, ClO, $Cl_y$, and $ClONO_2$ in the ER-2 data. The agreement between predicted and observed mixing ratios of HCl, $O_3$, ClO, $Cl_y$, and $ClONO_2$ are quite good for this particular flight. The HALOE air mass calculations capture the rapid decline in $O_3$ observed by the ER-2 at the edge of the vortex very well. The filament of vortex edge air is seen as high $O_3$, ClO, $Cl_y$, and $ClONO_2$ near 55° S in the air mass mixing ratios. The predicted water vapor mixing ratios, although low, capture the dehydration within the interior of the polar vortex. The agreement between the inferred $Cl_y$ and $ClONO_2$ is quite good, this suggests that the initial chlorine partitioning in the photochemical model is reasonable. High HCl and low ClO mixing ratios are associated with low $O_3$ mixing ratios within the interior of the vortex. This is a consequence of the rapid conversion of ClO and $ClONO_2$ into HCl as the polar vortex recovers in the late Antarctic spring. *Grooss et al.* [this issue] examines the role of the low $O_3$ mixing ratios in the Antarctic springtime chlorine deactivation in more detail.

## Conclusions

High-resolution in situ data from instruments onboard the ER-2 and contemporaneous HALOE observations of southern hemisphere middle latitudes during ASHOE/MAESA 1994 have been used to quantitatively evaluate the effectiveness of using a trajectory/photochemical box model to predict the dynamical and photochemical evolution of air masses observed by HALOE and thereby link the satellite and in situ observations of photochemically active species in the lower stratosphere. Statistical analysis of the agreement between predicted and observed concentrations of $HO_2$, HCl, $H_2O$, ClO, $O_3$, OH, $NO_y$, $CH_4$, and NO along ER-2 flight paths during the second (May-June) and fourth (October) deployments was performed for coincident HALOE trajectories.

The statistical tests support the hypothesis that the distribution of mixing ratios predicted HALOE trajectory/ photochemical box model are identical to the distribution observed by the ER-2 (averaged within the coincidence window) at the 0.05 significance level for $HO_2$, ClO, $O_3$, $NO_y$, $CH_4$, and NO. The statistical tests also support the hypothesis that the

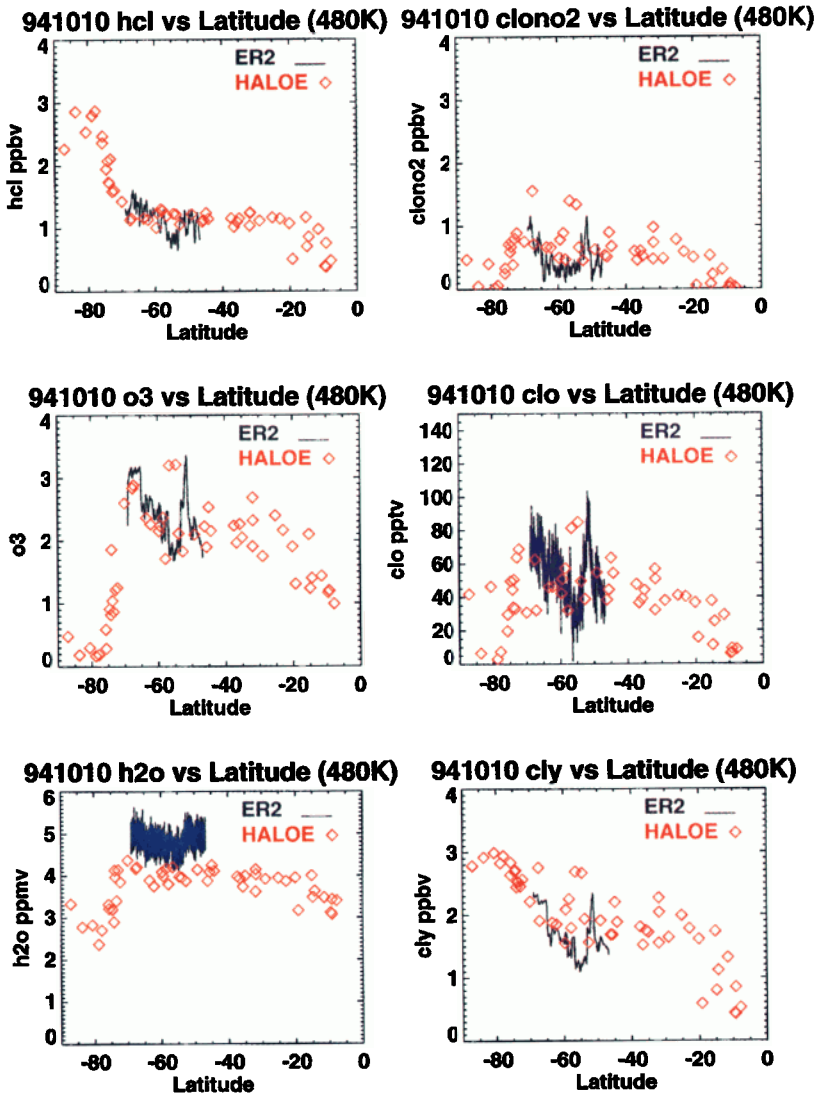


**Plate 1.** Observed and predicted distributions of HCl, $O_3$, $H_2O$, ClO, and inferred distributions of $Cl_y$ and $ClONO_2$ plotted as a function of latitude for the 941010 flight. Predicted concentrations of trace species on the 480 K isentropic surface at 0000 GMT on 941010 in a longitude band between 150° E and 150° W are shown as red diamonds. The ER-2 data is shown as a blue line and has been restricted to those observations with potential temperatures between 460 and 500 K.

predicted and observed variances within the distributions are identical at the 0.05 significance level for all species considered. However, the tests establish with 95% confidence that there are mean low bias in the predicted concentrations of HCl, $H_2O$, and OH mixing ratios of 0.09 ppbv, 0.68 ppmv, and 0.09 pptv, respectively.

The KS test, which measures the overall agreement between two sample distributions, was used to quantify the agreement between the predicted and the observed distribution of species along the ER-2 flight path. The actual KS significance levels were less than 0.50 for all species considered except ClO (KS=0.915), and consequently there is a strong likelihood (greater than 50%) of a Type II error (accepting the hypothesis when it should be rejected). The KS significance levels were generally much higher when the mean biases between the predicted and observed distributions are removed. dKS significance levels are greater then 0.80 (less than 20% chance of Type II error) for $H_2O$, ClO, $O_3$, and $NO_y$.

An analysis of the sources of errors in the predictions indicates that numerical trajectory errors are not the primary determinate of the KS significance levels for the number of coincidences obtained during the second and fourth ASHOE/MAESA deployments. Instead, uncertainty in the initial HALOE measurement accounts for the majority of the difference between the predicted and the observed distributions for all species. Overall, the results of this intercomparison suggest that the trajectory/box model calculation successfully carried the information contained in the initial HALOE observations forward in time to the ER-2 flight track and even added useful information about the global distribution of ClO, $ClONO_2$, and $Cl_y$. This study shows that the trajectory/box model predictions are a useful tool for linking satellite and in situ observations of the lower stratosphere.

**Acknowledgments.** The authors wish to acknowledge the ER-2 instrument PIs; Roland Chan, Chris Webster, Randy May, Jim Anderson, Rick Stimple, Paul Wennberg, David Fahey, Mike Proffitt, and Ken Kelly, for providing the in situ measurements which made this comparison possible. Thanks to Terry Davies for providing the UKMO operational forecasts and analyses during the ASHOE/MAESA deployments. A special thanks to Richard Winkler and Susan Hovde for their outstanding efforts in coordinating the retrieval of forecast and analysis products in Christchurch, New Zealand, and also to the HALOE data processing team at NASA Langley Research Center for providing near-real-time HALOE observations during the ASHOE/MAESA deployments. This research has been supported by the NASA MTPE EOS Interdisciplinary Science Program (PI, Grose) and the NASA Atmospheric Chemistry Modeling, and Analysis Program (PI, Pierce).

## References

Anderson, J. G., W. H. Brune, M. H. Proffitt, Ozone destruction by chlorine radicals within the Antarctic vortex: Spatial and temporal evolution of ClO-$O_3$ Anticorrelation based on in situ ER-2 data, *J. Geophys. Res., 94,* 11,465-11,479, 1989.

Austin, J., R. C. Pallister, J. A. Pyle, A. F. Tuck, and A. M. Zavody, Photochemical model comparisons with LIMS observations in a stratospheric trajectory coordinate system. *Q. J. R. Meteorol. Soc., 113,* 361-392, 1987.

Bacmeister, J. T., S. D. Eckerman, P. A. Newman, L. Lait, K. R. Chan, M. Loewenstein, M. H. Proffitt, and B. L. Gary, Stratospheric horizontal wavenumber spectra of winds, potential temperature and atmospheric tracers observed by high-altitude aircraft, *J. Geophys. Res., 101,* 9441-9470, 1996.

Bruhl, C. and P.J. Crutzen, MPIC two-dimensional model, in *The Atmospheric Effect of Stratospheric Aircraft*, edited by M.J. Prather and E.E. Remsberg, p. 103-104, NASA Ref. Publ. 1292, 1993.

Bruhl, C., et al., Halogen Occultation Experiment ozone channel validation, *J. Geophys. Res., 101,* 10,217-10,240, 1996.

Carslaw, K.S., S.L. Clegg, and P. Brimblecombe, A thermodynamic model of the system HCl-$HNO_3$-$H_2SO_4$-$H_2O$, including solubilities of HBr, from 328 K to < 200 K, *J. Phys. Chem., 99,* 11557-11574, 1995a.

Carslaw, K.S., B.P. Luo and T. Peter, An analytical expression for the composition of aqueous $HNO_3$-$H_2SO_4$-$H_2O$ stratospheric aerosols including gas phase removal of $HNO_3$, *Geophys. Res. Lett., 22,* 1,877-1,880, 1995b.

Chan, K. R., S. G. Scott, T. P. Bui, S. W. Bowen, and J. Day, Temperature and horizontal wind measurements on the ER-2 aircraft during the 1987 Airborne Antarctic Ozone Experiment, *J. Geophys. Res., 94,* 11,573-11,588, 1989.

Crutzen, P. J., J.-U. Grooss, C. Bruhl, R. Muller, and J. M. Russell III, A reevaluation of the ozone budget with HALOE UARS data: No evidence for the ozone deficit, *Science, 268,* 705-708, 1995.

Curtis, A. R., and W. P. Sweetenham, *Facsimile/Checkmat Users Manual*, 135 pp., Computer Sci. Sys. Div., Harwell Lab., Oxford, 1987.

DeMore, W. B., et al., Chemical kinetics and photochemical data for use in stratospheric modeling, *JPL publ. 94-26,* 273 pp, Pasadena, 1994.

Eluszkiewicz, J., and M. Allen, A global analysis of the ozone deficit in the upper stratosphere and lower mesosphere, *J. Geophys. Res., 98,* 1069-1082, 1993.

Fahey, D. W., K.K. Kelly, G. V. Ferry, L. R. Poole, J. C Wilson, D. M. Murphy, and K. R. Chan, In situ measurements of total reactive nitrogen, total water, and aerosol in a polar stratospheric cloud in the Antarctic, *J. Geophys. Res., 94,* 11,299-11,315, 1989.

Fairlie, T. D., R. B. Pierce, W. L. Grose, and G. Lingenfelser, Lagrangian forecasting during ASHOE: Analysis of predictive skill for analyzed and reverse-domain-filled potential vorticity, *J. Geophys. Res.*, this issue.

Gear, C. W., The automatic integration of ordinary differential equations, *Numer. Math., 14,* 176-179, 1971.

Gibbons, J. D., Nonparametric methods for quantitative analysis, in *American Series in Mathematical and Management Sciences*, 2nd ed., Vol. II, Am. Sci. Press, Columbus, Ohio, 1985.

Gidel, L.T., P.J. Crutzen, and J. Fishman, A two-dimensional photochemical model of the atmosphere; 1: Chlorocarbon emissions and their effect on stratospheric ozone, *J. Geophys. Res., 88,* 6622-6640, 1983.

Gordley, et al., Validation of nitric oxide and nitrogen dioxide measurements made by the Halogen Occultation Experiment for UARS platform, *J. Geophys. Res., 101,* 10,241-10,266, 1996.

Grooss, J.U., T. Peter, C. Bruhl and P.J. Crutzen, The influence on high flying aircraft on polar heterogeneous chemistry, in *Proceedings of the International Scientific Colloquium, Dtsch. Forschungs. fur Luft und Raumfahrt Mitteilung*, Cologne Germany, June, 1994.

Grooss, J. U., R. B. Pierce, P. J. Crutzen, William L. Grose, J. M. Russell III, Reformation of chlorine reservoirs in southern hemisphere polar spring. *J. Geophys. Res.*, this issue.

Hanson, D.R., and A.R. Ravishankara, Reactive uptake of $ClONO_2$ onto sulfuric acid due to reaction with HCl and $H_2O$, *J. Phys. Chem., 98,* 5728-5735, 1994.

Harries, J. E., J. M. Russell III, A. F. Tuck, L. L. Gordley, P. Purcell, K. Stone, R. M. Bevilacqua, M. Gunson, G. Nedoluha, and W. A. Traub, Validation of measurements of water vapor from the Halogen Occultation Experiment (HALOE), *J. Geophys. Res., 101,* 10,205-10,216, 1996.

Lary, D. J., and J. A. Pyle, Diffusive radiation, twilight and photochemistry, *J. Atmos. Chem., 13,* 373-406, 1991.

Lateltin, E., J.-P. Pommereau, H. Le Texier, M. Pirre, and R. A. Ramaroson, Perturbation of stratospheric nitrogen dioxide by volcanic aerosol in the arctic, *Geophys. Res. Lett., 21,* 1411-1414, 1994.

Loewenstein, M. J., J. R. Podolske, K. R. Chan, and S. E. Strahan, Nitrous oxide as a dynamical tracer in the 1987 Airborne Antarctic Ozone Experiment, *J. Geophys. Res., 94,* 11,589-11,598, 1989.

Lutman, E. R., J. A. Pyle, R. L. Jones, D. J. Lary, A. R. MacKenzie, and I. Kilbane-Dawe, Trajectory model studies of $ClO_x$ activation during the 1991/92 northern hemispheric winter, *Geophys. Res. Lett., 21,* 1419-1422, 1994.

Kelly, K. K., et al., Dehydration in the lower Antarctic stratosphere during late winter and early spring, 1987, *J. Geophys. Res., 94,* 11,317-11,357, 1989.

McElroy, M. B., and R. J. Salawitch, Stratospheric ozone: Impact of human activity, *Planet. Space Sci., 37,* 1653-1672, 1989.

Muller, R., and P.J. Crutzen, A possible role of galactic cosmic rays in chlorine activation during polar night, *J. Geophys. Res., 98,* 20,483-20,490, 1993.

Muller, R., T. Peter, P. J. Crutzen, H. Oelhaf, G. P. Adrian, Th. V. Clarmann, A. Wegner, U. Schmidt, D. Lary, Chlorine chemistry and the potential for ozone depletion in the Arctic stratosphere in the winter of 1991/92, *Geophys. Res. Lett., 21,* 1427-1430, 1994

Muller, R., P. J. Crutzen, J.-U. Grooss, C. Bruhl, J. M. Russell III, and A. F. Tuck, Chlorine activation and ozone depletion in the Arctic vortex: Observations by the Halogen Occultation Experiment on the Upper Atmosphere Research Satellite, *J. Geophys. Res., 101,* 12,531-12554, 1996)

Natarajan, M., and L. B. Callis, Examination of stratospheric ozone photochemistry in light of recent data, *Geophys. Res. Lett., 16,* 473-476, 1989

Natarajan, M., and L. B. Callis, Stratospheric photochemical studies with Atmospheric Trace Molecule Spectroscopy (ATMOS) measurements, *J. Geophys. Res., 96,* 9361-9370, 1991.

Park, J. H., et al., Validation of Halogen Occultation Experiment $CH_4$ measurements from the UARS, *J. Geophys. Res., 101,* 10,183-10,204, 1996.

Pfister, L., K. R. Chan, T. P. Bui, S. W. Bowen, M. Legg, B. L. Gary, K. K. Kelly, M. H. Proffitt, and W. Starr, Gravity waves generated by a tropical cyclone during the STEP tropical field program: A case study, *J. Geophys. Res., 98,* 8611-8638, 1993.

Pierce, R. B., and T. D. A. Fairlie, Chaotic advection in the stratosphere: Implications for the dispersal of chemically perturbed air from the polar vortex, *J. Geophys. Res., 98,* 18,589-18,595, 1993.

Pierce, R. B., W. L. Grose, J. M. Russell III, and A. F. Tuck, Evolution of southern hemisphere spring air masses observed by HALOE, *Geophys. Res. Lett., 21,* 213-216, 1994.

Pratt, J. W., and J. D. Gibbons, *Concepts of Nonparametric Theory,* Springer-Verlag, New York, 1981.

Proffitt, M. H., et al., In situ ozone measurements within the 1987 ozone hole from a high-altitude ER-2 aircraft, *J. Geophys. Res., 94,* 16547-16556, 1989.

Russell, J. M., et al., Validation of hydrogen chloride measurements made by the Halogen Occultation Experiment from the UARS platform, *J. Geophys. Res., 101,* 10,151-10,162, 1996.

Salawitch, R. J., et al., The distribution of hydrogen, nitrogen, and chlorine radicals in the lower stratosphere: Implications for changes in $O_3$ due to emission of $NO_y$ from supersonic aircraft, *Geophys. Res. Lett., 21,* 2547-2550, 1994.

Siskind, D. E., B. J. Connor, R. S. Eckman, E. E. Remsberg, J. J. Tsou, and A. Parrish, An intercomparison of model ozone deficits in the upper stratosphere and mesosphere from two data sets, *J. Geophys. Res., 100,* 11,191-11,201, 1995.

Webster, C. R., R. D. May, D. W. Toohey, L. M. Avallone, J. G. Anderson, P. Newman, L. Lait, M. R. Schoeberl, J. W. Elkins, and K. R. Chan, Chlorine chemistry on polar stratospheric cloud particles in the Arctic winter, *Science, 261,* 1130-1134, 1993.

Webster, C. R., R. D. May, C. A. Trimble, R. G. Chave, and J. Kendall, Aircraft Laser Infrared Absorption Spectrometer (ALIAS) for in-situ stratospheric measurements of HCl, $N_2O$, $CH_4$, $NO_2$, and $HNO_3$, *Appl. Opt., 33,* 454-472, 1994.

Wennberg, P. O. T. F. Hanisco, R. C. Cohen, R. M. Stimpfle, L. B. Lapson, and J. G. Anderson, In situ measurements of OH and $HO_2$ in the upper troposphere and stratosphere, *J. Atmos. Sci., 52,* 3413-3420, 1995.

R. Bradley Pierce and William L. Grose, NASA Langley Research Center, Mail Stop 401B, Hampton, VA 23681. (e-mail: r.b.pierce@larc.nasa.gov; grose@haloe.larc.nasa.gov)

Jens-Uwe Grooss, Forschungszentrum Juelich ICG-1 52425 Juelich, Germany. (j.-u.grooss@kfa-juelich.de)

James M. Russell III, Department of Physics, Hampton University, Hampton, VA 23668 (jmr@cs.hamptonu.edu)

Paul J. Crutzen, Chemie der Atmosphare, Max-Planck-Insitut fur Chemie, Postfach 3060 D-6500 Mainz, Germany (e-mail: air@mpch-mainz.mpg.d400.de)

T. Duncan Fairlie, Science and Technology Corporation, Hampton, VA 23666. (e-mail: t.d.fairlie@larc.nasa.gov)

Gretchen Lingenfelser, Science Applications International Corp., Hampton, VA 23666. (e-mail: g.s.lingenfelser@larc.nasa.gov)

(Received March 13, 1996; revised October 22, 1996; accepted October 24, 1996.)